RESEARCH PAPER

Nucleus 5:5, 449–461; September/October 2014; © 2014 Landes Bioscience

Distinct chromatin signature of histone H3 variant H3.3 in human cells

Luc Snyers[†], Gordin Zupkovitz[†], Marlene Almeder, Marianne Fliesser, Anja Stoisser, Klara Weipoltshammer, and Christian Schöfer*

Department for Cell and Developmental Biology; Medical Imaging Cluster; Medical University of Vienna; Vienna, Austria

[†]These authors contributed equally to this work.

Keywords: histones, nuclear architecture, chromatin, transcription, superresolution imaging

Abbreviations: FISH, fluorescent in-situ hybridization; DAPI, 4',6-diamidino-2-phenylindole; HSA, *Homo sapiens*; BrUTP, bromo-UTP; PBS, phosphate buffered saline; SSC, saline-sodium citrate

Actively transcribed regions of the genome have been found enriched for the histone H3 variant H3.3. This variant is incorporated into nucleosomes throughout the cell cycle whereas the canonical isoforms are predominately deposited in association with replication. In order to obtain a global picture of the deposition pattern at the single cell level we expressed H3.3 in both normal and malignant human cells and analyzed nuclei using conventional and structured illumination imaging (SIM). We found that the distribution pattern of H3.3 in interphase differs from that of the canonical histone H3 variants and this difference is conveyed to mitotic chromosomes which display a distinct H3.3 banding pattern. Histone H3.3 localization positively correlated with markers for transcriptionally active chromatin and, notably, H3.3 was almost completely absent from the inactive X chromosome. Collectively, our data show that histone variant H3.3 occupies distinct intranuclear chromatin domains and that these genomic loci are associated with gene expression.

Introduction

In interphase nuclei the genome is distributed in a non-random fashion reflecting the major nuclear functions. The genomic DNA forms complexes with proteins which represent not only important structural components of chromatin but exert prominent regulatory control functions on the genome such as transcriptional activation or repression, which is reflected in the intranuclear extent and distribution pattern of the respective chromatin compartments. Core histones building up the nucleosomes are the main constituents of chromatin and changes in properties of histones impart epigenetic regulation of gene expression. Apart from post-translational histone modifications histone replacement is an important factor adding another layer of complexity to the regulation of gene expression.

The majority of histones, usually referred to as canonical histones, is expressed and assembled to form nucleosomes during S-phase of the cell cycle ensuring propagation of chromatin and epigenetic marks to the daughter cells. Histones H3.1 and H3.2 represent the canonical H3 histones; however, several further H3 isoforms are known. The expression of five of them is tissue-specific (H3T, H3.X, H3.Y, and H3.5) or specific for centromeric regions of the genome (CENP-A, also termed CenH3). The histone H3 variant H3.3 has recently received much attention as its deposition into nucleosomes has been associated with transcriptional activity.[1,2] Further support for the association of H3.3 replacement with transcription was lent by the facts that H3.3 is ubiquitously expressed throughout the cell cycle,[3] becomes enriched in post-mitotic neurons,[4] is incorporated in activated inducible (trans-) genes[5-7] and correlates with markers for transcriptionally active chromatin.[2,8,9]

While H3.3 was recently also detected in pericentric[10-13] and telomeric[14-16] chromatin, identification of H3.3 at a genome-wide level confirmed preferential association with active gene bodies.[16-19] H3.3 incorporation was also detected in promoter and enhancer sequences with controversial findings reported in relation to the transcriptional activity of the respective genes.[16,20-24]

Genome-wide studies as well as proteomic studies[25] demonstrated nuclear distribution patterns of H3.3 which are different from those of canonical H3 in the genome of mammalian cells. In this respect it is interesting, that H3.3 differs from H3.2 only in four and from H3.1 in five amino acid residues. Selectivity in deposition control is achieved by histone- and site-specific chaperones. The death-associated protein (DAXX) together with the α-thalassemia and/or mental retardation X-linked syndrome protein (ATRX) deposits H3.3 in pericentric[11] and telomeric regions[14-16] during S-phase. In euchromatic regions H3.3 deposition is mediated by the

*Correspondence to: Christian Schöfer; Email: christian.schoefer@meduniwien.ac.at
Submitted: 03/04/2014; Revised: 08/21/2014; Accepted: 08/25/2014; Published Online: 08/25/2014
http://dx.doi.org/10.4161/nucl.36229

chaperone Histone regulator A (HIRA)[26,27] throughout the cell cycle.

Although strongly associated with transcriptional activity it is currently under debate whether H3.3 is a prerequisite or a consequence of transcription, if it is required for maintaining a chromatin conformation suitable for transcription or if it rather represents a general replacement histone after histone eviction.[28]

Interestingly, knockout studies demonstrated that loss of H3.3 is compatible with viability[29-33] nevertheless, it has become clear that H3.3 is important for embryogenesis[34-40] (for reviews see refs. 41–43) and is enriched at developmentally regulated genes.[16,36] Intriguingly, in an increasing number of malignancies deregulation of H3.3 incorporation has recently been found and discussed as possible patho-mechanism[44-50] (for reviews see refs. 51 and 52).

Most studies on H3.3 distribution applied molecular methods, which collect data of many cells or entire tissue blocs. In this study we investigated the distribution pattern of the histone H3 variant H3.3 at the single cell level in both normal and malignant human cells. We expressed an N-terminally truncated H3.3 construct incompetent of replication-dependent incorporation into nucleosomes,[2] thus enabling the study of fast cycling cells. The H3.3 topology was correlated with nuclear components and furthermore, the distribution of H3.3 was analyzed with respect to canonical H3. Finally, we evaluated mitotic chromosomes in order to see if a specific interphase topology of H3.3 was transmitted to mitotic chromatin. Cells were analyzed by conventional microscopy and high-resolution structured illumination imaging.

Results

Distribution of histone H3.3 in interphase nuclei

In our study we decided to make use of a mCherry-fused N-terminally truncated H3.3 construct (hereafter named H3.3-ΔN) for expression in fast cycling cells because H3.3-ΔN has previously been shown to be replication-incompetent[2] allowing us to focus on nucleosomal deposition associated with transcriptional activity. It is important to note that we found no significant differences in the expression patterns of H3.3-ΔN and full-length H3.3 at the level of microscopy (**Fig. 1**; see Materials and Methods). Transient expression of the mCherry-fused N-terminally truncated H3.3 construct led to a predominantly nuclear distribution of signal (see e.g., **Fig. 2A′′, B′, and C′′**). In a first step we correlated H3.3-ΔN (**Fig. 2A′′**) with HIRA (**Fig. 2A′**). HIRA is the histone chaperone specifically targeting H3.3 to transcriptionally active or transcriptionally competent loci. We found a high degree of co-localization between the two signals (**Fig. 2A′′′**). Next, we compared the expression profile of H3.3-ΔN with markers for transcriptionally silent chromatin, such as DAPI (**Fig. 2B**), and found largely exclusive staining patterns (**Fig. 2B′′ and B′′′**). In contrast, correlation of H3.3-ΔN expression (**Fig. 2C′′**) with BrUTP incorporation into nascent RNA as a marker for transcription (**Fig. 2C′**) resulted in a significant signal overlap (**Fig. 2C′′′**). Similarly, H3.3-ΔN and H3K4me3, a histone modification characteristic of transcriptionally active chromatin, were largely overlapping (not shown). Together our data on the nuclear topology of H3.3-ΔN demonstrate that the distribution of the replication-incompetent pool of H3.3 correlates positively with markers for transcriptional activity. In this respect our data confirm previous results expressing full-length constructs of H3.3 in *Drosophila* cells and recent studies on H3.3 in human mesenchymal stem cells,[2,19,53] and extend the data to normal and malignant human cells.

Correlation of H3.3 topology with nuclear compartments

Chromosome territories

One of the major nuclear compartments are the chromosome territories (CTs) representing the interphase correlates of mitotic chromosomes. We performed FISH with a chromosome 6 (HSA6)-specific painting probe in Hela cells expressing H3.3-ΔN. On average 3 CTs per cell were labeled and distinct bright foci became visible within the volume of CTs after FISH (**Fig. 3A**). These are believed to be domains of about 1 Mbp size representing transcriptionally inactive chromatin with transcription occurring around these domains.[54,55] The overlay of H3.3-ΔN and FISH (**Fig. 3A-A′′′′**) did not reveal any preferences in signal distribution within the respective CT. No significant difference in H3.3-ΔN distribution could be observed between the inside and outside of the CTs. When comparing the spatial relation of H3.3-ΔN with the bright dots after FISH we could observe that indeed the signal of H3.3-ΔN was adjacent to these dots with some overlap at the periphery (**Fig. 3A′′** inset). Similar results were obtained for other chromosomes including the X-chromosomes (not shown). Interestingly, in normal human female cells, we noticed that the inactive X chromosome, detected by immunolabeling H3K27me3 which is enriched in the Xi, was located in a nuclear volume with reduced signal for H3.3-ΔN (**Fig. 3B–B′′′**).

Nuclear speckles

Prominent nuclear compartments are nuclear speckles (also termed interchromatin granules) with its main constituent splicing factor SC-35. Nuclear speckles are involved in mRNA splicing and previous studies using conventional light and electron microscopy suggested that the interior of splicing speckles is devoid of transcriptionally active sequences. Close proximity of splicing speckles to euchromatic neighborhood was demonstrated[56] and subsequently association of actively transcribed genes with splicing speckles could be observed.[57] Our findings by using high-resolution SIM of cells expressing H3.3-ΔN are in line with these studies and a recent SIM study analyzing DAPI and immunostaining.[58] Using conventional confocal imaging we found that the areas positive for SC-35 were devoid of H3.3-ΔN signal (data not shown). Using SIM we frequently observed delicate H3.3-ΔN-positive strands entering the periphery of the SC-35 positive area. Larger magnifications show that small foci of SC-35 positive signal were found to lie in the vicinity of these H3.3-ΔN positive strands (**Fig. 3C–C′′′′**), thus indicating the presence of transcription at the interphase nuclear speckle and/or chromatin.

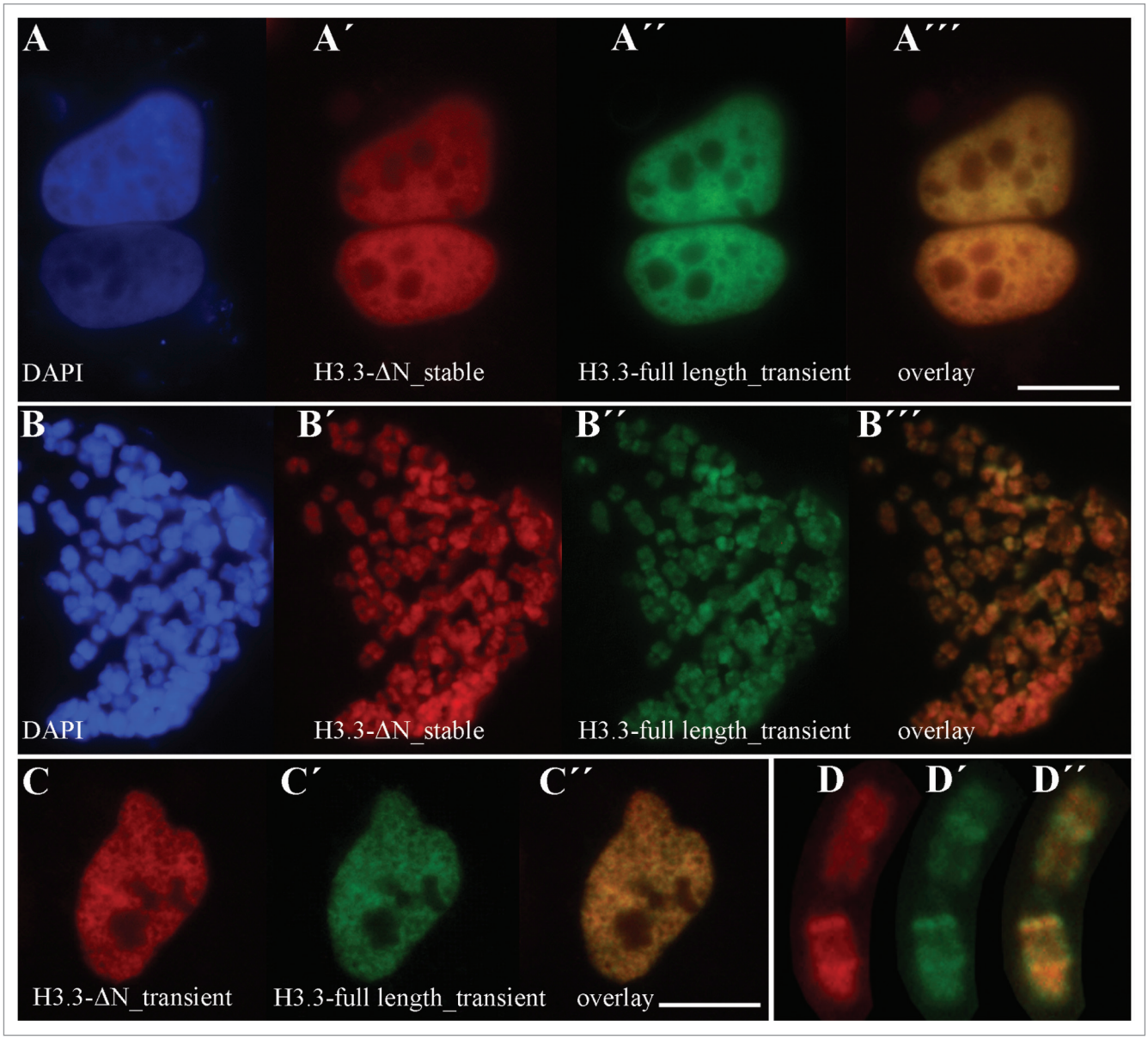

Figure 1. Comparison of expression patterns of full-length H3.3 with H3.3-ΔN in Hela cells; wide-field imaging. Expression patterns of transiently expressed full-length H3.3 (**A″, B″, D′**) co-localize well with the stably expressed H3.3 patterns (**A′, B′, D**) as seen in red and green channel overlays (**A‴, B‴, D″**) in interphase (**A–A‴**), metaphase (**B–B‴**), and single chromosomes with the example of HSA1 (**D–D″**); DNA staining with DAPI (**A, B**). Likewise, transient co-expression of both H3.3-ΔN (**C**) and full-length H3.3 (**C′**) displays significant co-localization in interphase nuclei (**C″**). Spearman's $r = 0.887$ in (**A‴**) and 0.914 in (**C″**). Scale bars, 10 μm.

Comparison of major histones H3 in interphase nuclei

After having studied the nuclear topology of histone H3.3-ΔN in relation to chromatin and to nuclear domains, we next addressed differences in nuclear deposition of the three major H3 histones H3.1, H3.2, and H3.3. We evaluated nuclei that co-express H3.3-ΔN together with either H3.1, H3.2. or H2B, the latter being present in both eu- and heterochromatic domains. We used 3-D SIM in order to obtain a high-resolution picture of the nuclear topology of the histones investigated.

Indeed, these histones showed significant differences in their localization patterns. When comparing histones H3.3-ΔN and H2B (**Fig. 4A–A‴**) we found little overlap in heterochromatic areas, such as in perinucleolar chromatin, which was positive for H2B but negative for H3.3-ΔN. We further concentrated on measuring co-localization in euchromatic regions which are the areas of ongoing gene expression. A considerable degree of co-localization could be observed in these areas (**Fig. 4A‴**). This visual impression is reflected in gray value profiles (**Fig. 4A⁗**) and, applied to larger volumes, in the co-localization coefficient measurement. As a measure of co-localization we calculated the Spearman's coefficient *r*, which ranges from -1 to +1 indicating complete contra- or co-localization. The latter method resulted in a Spearman's coefficient of $r = 0.665$ demonstrating good co-localization of the two signals in euchromatic areas. In

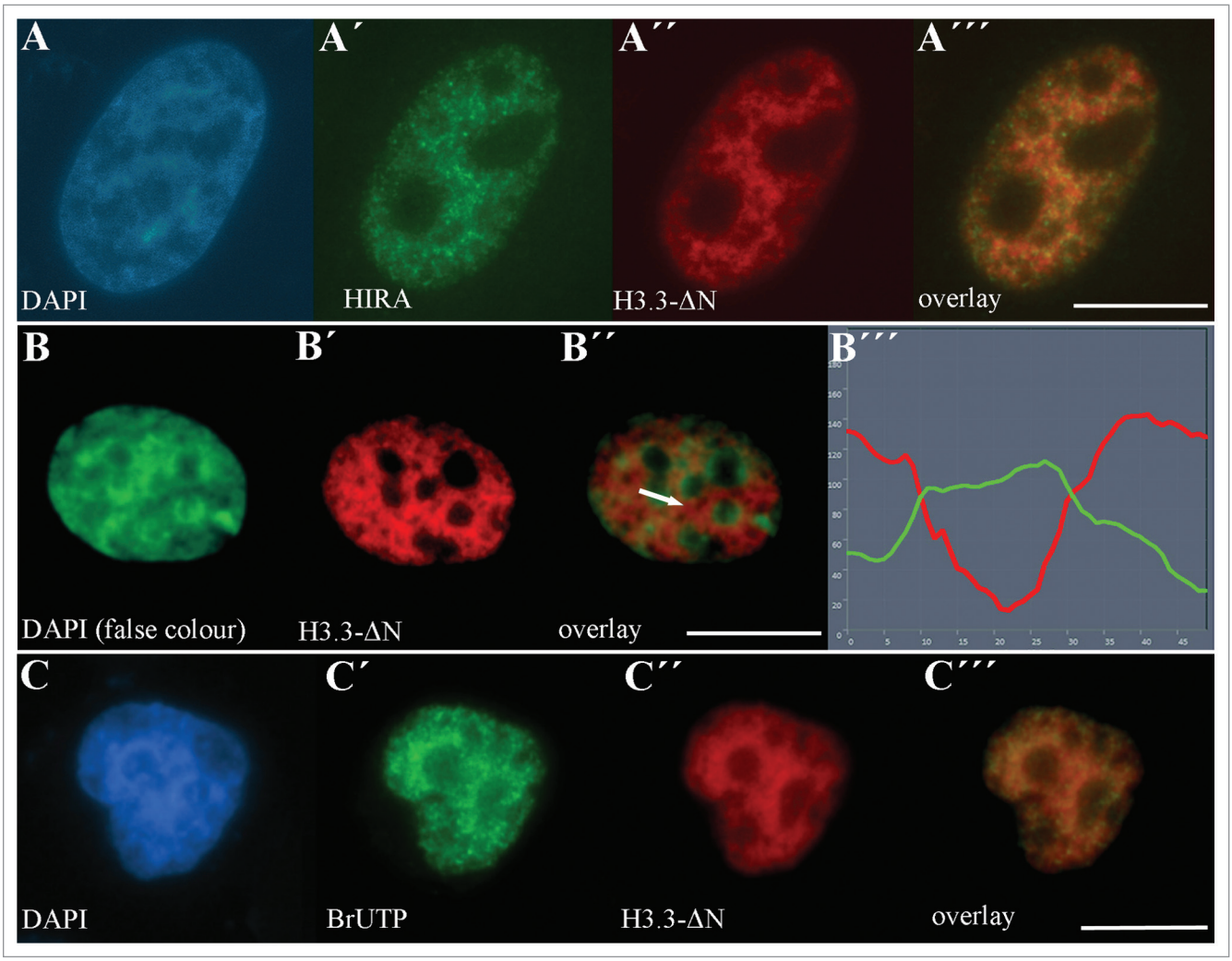

Figure 2. Expression pattern of histone variant H3.3-ΔN in interphase nuclei; wide-field imaging. Hela cell (**A-A‴**) immunostained for HIRA (**A′**) and expressing H3.3-ΔN (A″). Both patterns correlate well as seen in the red and green channel overlay (**A‴**; Pearson's $r = 0.816$); DNA is stained with DAPI (**A**). In HUVEC cells (**B-B‴**) heterochromatin is highlighted by DAPI staining (**B**; DAPI shown in green color); H3.3-ΔN expression pattern (**B′**), overlay in (**B″**). Note largely exclusive staining in heterochromatic areas; a representative gray value profile (arrow in **B″**) is displayed in (**B‴**). In Hela cells (**C-C‴**) newly synthesized RNA is labeled after incorporation of BrUTP into nascent transcripts (**C′**) and correlates well with expression of H3.3-ΔN (**C″**) as seen in the red and green channel overlay (**C‴**; Pearson's $r = 0.813$); DNA staining with DAPI (**C**). Scale bars, 10 μm.

contrast Spearman's coefficient was $r = 0.23$ in heterochromatic areas. Comparison of H3.3-ΔN with either H3.1 (**Fig. 4B–B‴**) or H3.2 (**Fig. 4C–C‴**) revealed that the correlation was markedly lower than the correlation H3.3/H2B euchromatic. This impression is mirrored in gray value profiles (**Fig. 4B‴′and C‴′**) and in the correlation coefficient measurements $r = -0.299$ comparing H3.3-ΔN with H3.1 and $r = 0.196$ comparing H3.3-ΔN with H3.2, which does not support significant co-localization. Together these data show that the distribution of H3.3 differs from the one of the canonical H3 histones in interphase nuclei of Hela cells.

Expression of H3 variants in mitotic chromosomes

The differential staining of the three H3 histone variants in interphase nuclei suggests that this pattern might be transmitted to mitotic chromosomes. For this purpose we chose to use cytospin preparations of chromosomes despite lower resolution than in conventional spread preparations. This way nucleosomal occupancy of mitotic chromosomes is maintained, which is not the case for acetic acid treated spread preparations. Indeed, in metaphase chromosomes a clear banding pattern was observed in cells expressing H3.3-ΔN (**Fig. 5A′**). These bands were negatively correlated with DNA staining dyes such as DAPI (**Fig. 5A, B, and B″**) or quinacrine mustard for Q-banding (**Fig. 5B–B″**), once more demonstrating the exclusive staining of H3.3-ΔN with markers for transcriptional silent chromatin. The observed banding pattern was consistently found at the same positions in the homologs of a particular metaphase plate (**Fig. 5B–B″**), in different metaphase chromosomes of the same cell type (not shown) and in the same chromosomes of different cell types (**Fig. 5B–B″**). Furthermore, when comparing chromosomes 18 (HSA18) and 19 (HSA19), which are of different gene density, we found that H3.3-ΔN signal is

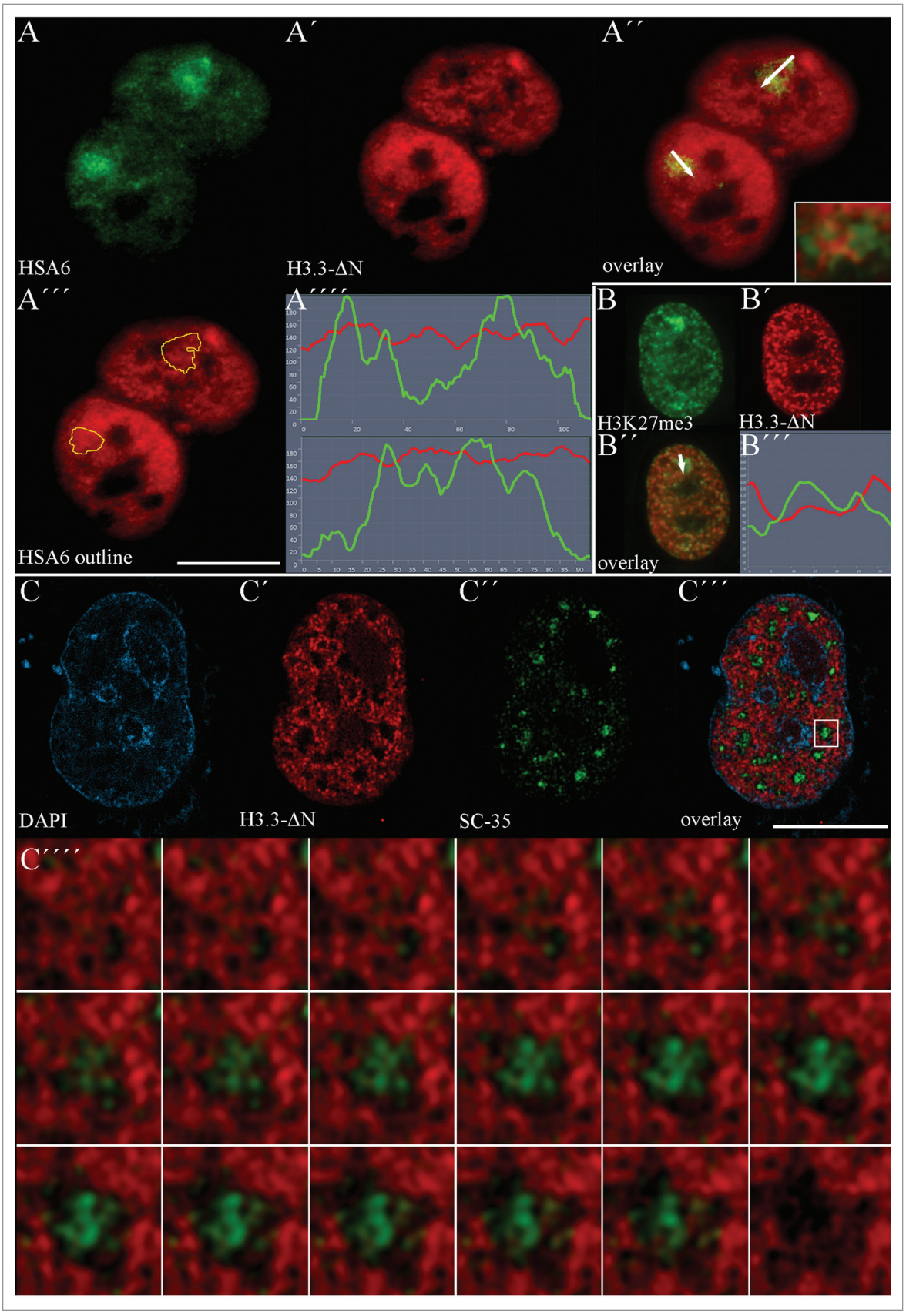

Figure 3. For figure legend, see page 454.

Figure 3 (See previous page). Distribution of histone H3.3-ΔN in relation to nuclear compartments in Hela (**A-A′′′; C-C′′′′**) and HUVEC (**B-B′′′**) cells; confocal sections (**A–B′′**) and SIM (**C–C′′′′**). H3.3-ΔN expressing cells (**A′**) were hybridized to depict chromosome territories (CTs) for HSA6 (**A**, FISH); overlay in (**A′′**) (inset: H3.3-ΔN signal is found at the periphery of bright FISH-dots). In (**A′′′**) the outline of the CTs were indicated (see Materials and Methods) and representative gray value profiles (arrows in **A′′**) are displayed in (**A′′′**). No significant change in H3.3-ΔN level can be seen in relation to the inner or outer parts of the CTs, nor between the CTs and the chromatin outside the depicted CT6. H3.3-ΔN expressing HUVEC cells (**B′**) were immunostained for H3K27me3 (**B**); overlay of H3.3-ΔN with H3K27me3 (**B′′**). Grey value profile (arrow in **B′′**) shows reduced H3.3-ΔN expression in the region of the inactive X chromosome (**B′′′**). Splicing speckles as indicated by detection of SC-35 (**C′′**) were correlated with H3.3-ΔN expression (**C′**) and DNA staining (**C**; DAPI); overlay of all three channels in (**C′′′**); structured illumination image, single confocal image plane. In (**C′′′′**) an area boxed in (**C′′′**) is displayed as *z*-stack. Small SC-35 positive foci become apparent at strands of H3.3-ΔN containing chromatin and coalesce to form large speckles which are devoid of H3.3-ΔN. Scale bars, 10 μm.

enriched in HSA19 (high gene density) as compared with HSA18 (low gene density; **Fig. 5B′′**).

We reasoned that the H3.3-ΔN banding pattern of chromosomes of a malignant cancer cell might differ from that of normal cells due to severely altered transcriptomes of malignant cells. However, when comparing chromosomes of Hela cells with little genomic rearrangements with the corresponding ones of normal cells (HUVEC) a similar banding pattern was observed (**Fig. 5B–B′′**). This suggests that the H3.3-ΔN bands observed in mitotic chromosomes represent larger genomic domains of actively expressed sequences and that transcriptional deregulation of smaller loci is likely to be below the sensitivity threshold of the method.

We found that H3K27me3, a marker for the inactive X chromosome occupied a region with reduced H3.3-ΔN signal intensity in interphase nuclei (**Fig. 3B′′′**). When we analyzed metaphase plates of normal female cells we could clearly identify the inactive X-chromosome because it was almost devoid of any H3.3-ΔN signal whereas the active X-chromosome displayed a banding pattern comparable to autosomal chromosomes (**Fig. 5C–C′′′′**).

Co-expression of H3.3-ΔN with canonical H3 histones in mitotic chromosomes revealed the mentioned banding pattern for H3.3 whereas H3.1 (**Fig. 5D–D′′**) or H3.2 (not shown) did not show similarly conspicuous bands.

These findings further confirm that H3.3-ΔN predominantly marks transcriptionally active chromatin. The results on mitotic chromosomes lead us to hypothesize that the H3.3-ΔN signal might reflect the previous interphase transcriptome at the single cell level.

Discussion

Molecular studies revealed differences in the distribution of canonical H3 and H3.3 at a genome wide level.[25] It has been proposed that the three H3 variants may represent epigenetic labels specific for euchromatin (H3.3), facultative (H3.2), and constitutive heterochromatin (H3.1). This differential distribution in interphase would then become visible in mitotic chromosomes, leading to a banding pattern indicative of a "H3 barcode"[59] and representing the structural requirements for the epigenetic memory effect.

In this study we used conventional and structured illumination imaging to study the distribution of H3.3 in nuclei of both normal and malignant human cells. The microscopic approach enabled us to study global chromatin arrangement at single cell level, to compare interphase and mitotic chromatin and to correlate it with nuclear components.

The data presented in this study support the view that H3.3 is preferentially associated with transcriptional activity. This is most clearly demonstrated by the differential signal in the Xa and the Xi (**Fig. 3B and 5C**), where Xa displays bands comparable to autosomal chromosomes, whereas Xi is almost devoid of signal. It remains to be determined if the very low level of fluorescence found in the Xi represents the genes escaping X-inactivation. Further support to a general association with transcriptional activity is caused by the negative correlation with dyes preferentially highlighting heterochromatin (DAPI, quinacrine mustard) and by the positive correlation with indicators of ongoing transcription, such as the detection of nascent transcripts by BrUTP (**Fig. 2B and C**). Recently, it has been shown that H3.3 is also incorporated into telomeric, pericentric and centromeric loci, in the latter of which a "placeholder" function of H3.3 was demonstrated.[60] In these regions the deposition of H3.3 was proposed to correlate with transcription during S-phase.[11] In our study, we did not find any significant incorporation of H3.3 into centromeric and pericentric regions. Reasons for this discrepancy may possibly be the requirement of the N-terminus of H3.3 or the modification(s) of its N-terminal residues for incorporation into these heterochromatic loci. Ongoing studies comparing deposition patterns of the full-length H3.3 construct and H3.3-ΔN will help to clarify this hypothesis.

In a recent study H3.3 has been co-expressed in human mesenchymal stem cells together with H3.2 and H2B.[19] Using wide-field fluorescence microscopy the authors reported partially overlapping H3.3 distribution with H2B and similar, yet non-identical distribution patterns between H3.3 and H3.2. Given the diameter of extended nucleosomal DNA of approximately 10 nm, microscopic evaluation evidently benefits from using high-resolution microscopic methods, which made us apply one of the novel high-resolution methods in order to study the nuclear H3.3 distribution pattern. Structured illumination imaging (SIM, also termed superresolution microscopy) lowers the resolution limit to nominally 100 nm in *x-y* and to 300 nm in *z* and has recently been successfully used to study nuclear architecture.[61,62] Using SIM together with quantification of co-localization by calculating the Pearson's correlation coefficient, we could show that at this level of resolution no significant overlap of the H3.3 with either H3.1 or H3.2 signals exists, whereas the co-localization was much more prominent when comparing H3.3 with H2B.

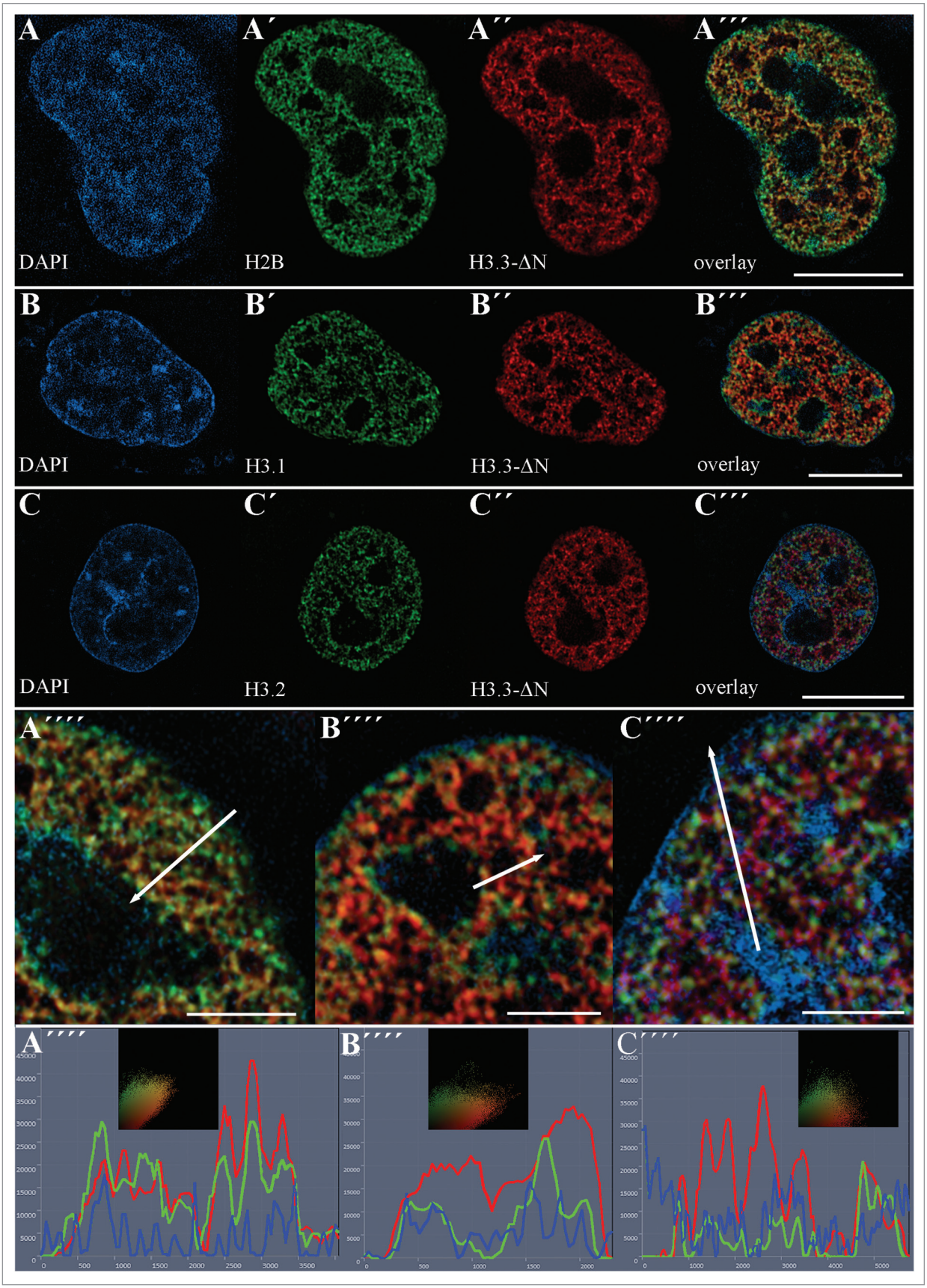

Figure 4. For figure legend, see page 456.

Figure 4 (See previous page). SIM imaging of Hela cell interphase nuclei co-expressing H3.3-ΔN and another histone; single confocal sections. DNA staining with DAPI (**A, B, C**), histones H2B (**A′**), H3.1 (**B′**), and H3.2 (**C′**); with H3.3-ΔN (**A′′, B′′, C′′**); overlay of all three channels in (**A′′′, B′′′, C′′′**). Enlarged areas of the overlay images are shown in (**A′′′′, B′′′′, C′′′′**) and corresponding gray value profiles are displayed below as indicated by arrows in (**A′′′′-C′′′′**). Embedded within the profile charts are scatterplots of the images (**A′′′, B′′′, C′′′**) to show entire pixel populations of H3.3 and one of the three other histones (abscissa: red channel [H3.3], ordinate: green channel). Scale bars, 10 μm and 3 μm (**A′′′′-C′′′′**).

In interphase individual chromosomes occupy distinct spaces within the nuclear volume termed chromosome territories (CTs). According to earlier studies, transcription is favored at the periphery of CTs but later it was shown that transcription may occur within CTs and is occurring at the periphery of foci of about 1 Mbp that become visible after FISH with whole-chromosome painting probes[63] (for a review see ref. 64). In line with these data we did not observe any specific enrichment or depletion of H3.3 at CT boundaries when correlated with CTs after FISH. However, our data support the view that transcriptional activity takes place at the periphery of the bright foci after FISH (**Fig. 3A′′** inset). In contrast, the CT of the inactivated X chromosome contained reduced H3.3 signal which correlates well with the metaphase staining pattern and, once again, points to a predominantly transcription-related expression pattern of H3.3-ΔN signal.

Another major nuclear component are the splicing speckles having been shown to associate at their periphery with active chromatin.[56] Correlation of H3.3 with splicing speckles showed that H3.3 positive chromatin strands enter just the periphery of the speckles. The association of active genes with speckles is mediated by promoter sequences[65] and it is thus tempting to speculate, that enrichment of H3.3 in promoters is involved in this association.

The differential distribution of H3.3 in relation to the canonical H3 histones in interphase nuclei emerged as distinct H3.3 banding pattern in mitotic chromosomes. The canonical histones H3 did not show bands similarly conspicuous as H3.3 did although the fluorescence was inhomogenously distributed over the length of chromosomes and appeared somewhat enriched at heterochromatic sites (**Fig. 5D′′**).

The distinct H3.3 bands were remarkably consistent even in homologous chromosomes of different human cell types, while the Xi in normal female cells was almost negative. The correlation of H3.3 and transcriptional activity is further supported by comparing HSA18 and HSA19. The two chromosomes have been used as models in studies evaluating the intranuclear position of chromosome territories[66] because of their marked difference in gene density. HSA18 is gene poor containing on average only 8.1 genes per Mbp, whereas HSA19 is gene rich harboring on average 36.3 genes per Mbp (NCBI annotation release 105). Transcriptome database search in untreated Hela cells revealed that the median value of transcript signal is 39.21 and 81.72 for HSA18 and HSA19, respectively. In agreement with the expression values our results clearly show that the H3.3 signal was significantly enriched in HSA19 as compared with HSA18 (**Fig. 5B``**).

Taking together all data, we hypothesize that these H3.3 positive bands correlate with the epigenetic memory of the transcriptome of the previous interphase of the cell.

Material and Methods

Cloning of constructs

For H3.3-ΔN the plasmid pPHSH3.3(Δ3–35) was used as template to amplify a fragment containing the truncated *Drosophila* H3.3 coding region (lacking 33 amino acids near the N-terminus and corresponding to construct $H3.3^{\Delta 335}$ as in ref. 2 Fig. 6). The amplicon was ligated in vector pcDNA3 modified to allow fusion with mCherry at the C-terminus of a protein, including a five amino acid linker. The resulting plasmid was used for transient transfection. For stable expression, H3.3-ΔN-mCherry was subcloned in vector pEF.Bos-puro. Puromycin-resistant clones were isolated and screened by fluorescent microscopy. Full-length H3.3 fused to GFP was excised from plasmid pPHSH3.3-GFP and ligated in expression vector pOPRSVI/MCS (Stratagene). Note that *Drosophil*a and human H3.3 differ at the level of nucleotides, but have identical amino acid sequences. For histone H3.1 the coding region was amplified from genomic DNA of HeLa cells using oligonucleotides 5′- atggctcgta cgaagcaaac agc-3′ and 5′- agccctctcg ccgcggatac g-3′. The resulting fragment was cloned in pCR4-TOPO (Life Technologies), and the sequence was verified. H3.1 was excised from this plasmid and ligated in pcDNA3 (Life Technologies) modified to allow fusion of YFP at the C-terminus of a protein, including an eight amino acid linker. For histone H3.2 the coding region was amplified from an IMAGE clone (IMAGE: 30915509) using oligonucleotides 5′- atggcccgta ctaagcagac -3′ and 5′- agcccgctct ccacggatgc -3′, cloned in PCR4-TOPO, and subsequently fused to YFP in vector pcDNA3. All constructs were verified by dideoxysequencing. The plasmid pcDNA3. H2Bj-YFP was obtained from the Department of Biomedical Sciences, University of Padova, Padova, Italy.

Cell culture and transfection

Hela cells (cervical cancer) were used as an example for a malignant cell type and human endothelial umbilical vein cells (HUVEC) as normal cells with a female karyotype.

Cells were grown on coverslips placed in 12-well plates in Dulbecco's Modified Eagle's Medium (DMEM, Sigma) under 5% $C0_2$ at 37 °C and supplemented with 10% fetal bovine serum (FBS; Sigma). Transient transfection of either mCherry-H3.3-ΔN alone or co-transfection with either YFP-H3.1, YFP-H3.2, YFP-H2B, or the full-length GFP-H3.3 was performed using lipofection (Lipofectamine, Life technologies) according to the manufacturer's instructions for Hela cells. After 4–6 h the transfection medium was replaced by growth medium for 10–14 h before further treatment. For studying interphase nuclei, cells were briefly washed in PBS buffer, fixed in 4% paraformaldehyde (PFA)/ PBS for 20 min at 10 °C and further washed in PBS at room temperature. Cells were then either counterstained with DAPI or subjected to further treatments.

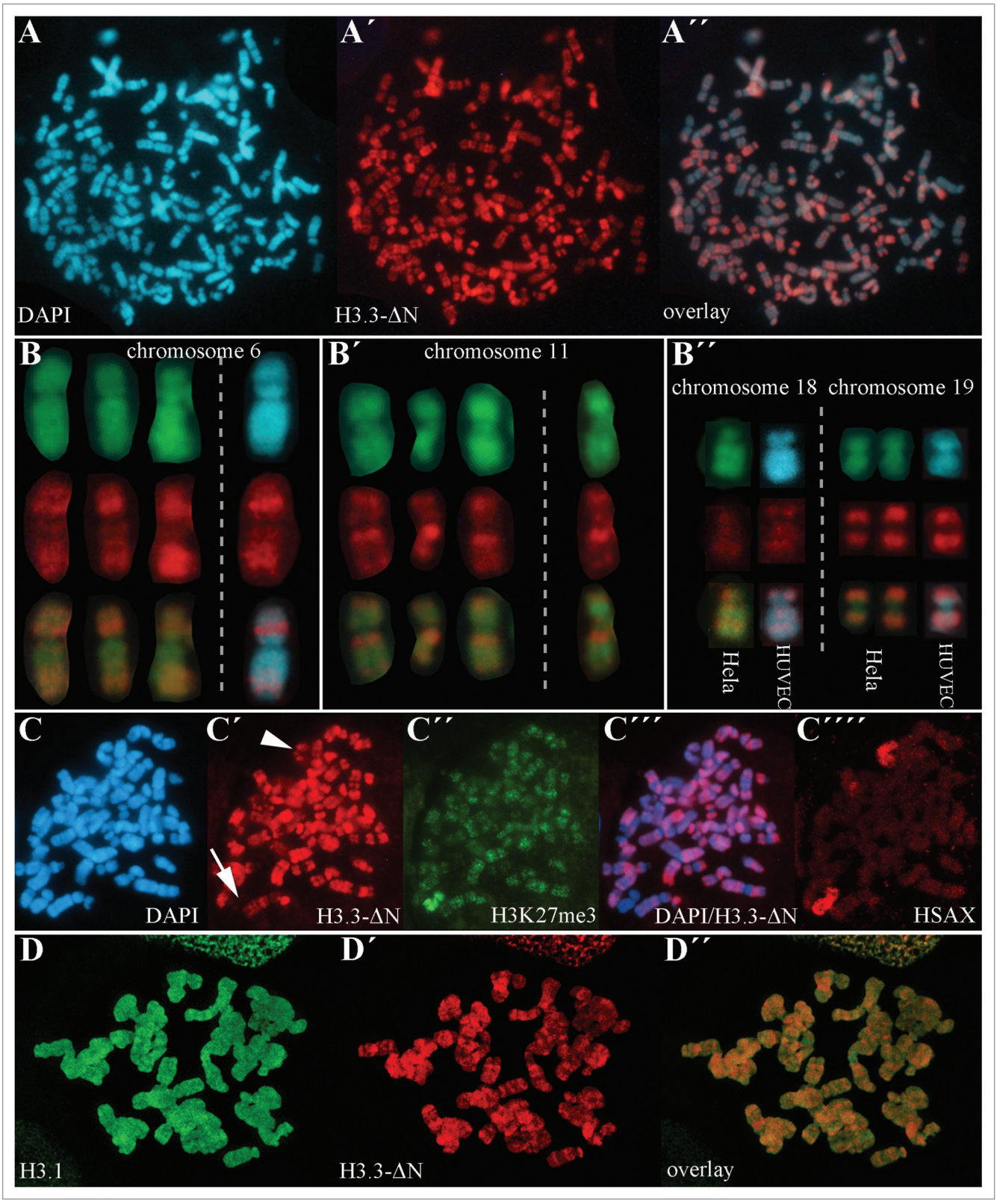

Figure 5. For figure legend, see page 458.

For the detection of nascent RNA molecules H3.3-ΔN expressing cells were incubated with 5-Bromouridine 5′-triphosphate (BrUTP) for 30 min as previously described.[67] Briefly, cells were incubated in streptolysin O, washed in PBS

Figure 5 (See previous page). Distribution of H3.3-ΔN in mitotic chromosomes in Hela (**A-B′′, D–D′′**) and HUVEC cells (**B-C′′′′**); wide-field imaging (**A–C′′′′**) and SIM (**D–D′′**). Cytospin of a metaphase plate stained for DNA (DAPI; **A**) and expressing H3.3-ΔN as distinct bands along chromosomes (**A′**; overlay **A′′**). Pictures of homologs of HSA6, HSA11, HSA18 and HSA19 (**B-B′′**) of the same metaphase plate (Hela cells) with homologs of HUVEC cells, as indicated. DNA stained either with quinacrine mustard (Q-banding, green; top row) or with DAPI (blue, top row); middle row expression of H3.3-ΔN and lower row overlay. In (**B**) left the three copies of Hela HSA6 are depicted and on the right side one copy of HUVEC chromosome 6 (note that Hela cells are aneuploid, whereas HUVEC cells have a normal set of chromosomes) and in (**B′**) another example is shown for HSA11 (left Hela; right HUVEC). In (**B′′**) HSA18 and HSA19 of Hela and HUVEC cells are compared which differ in gene density and global gene expression levels albeit they are of similar sizes. In all cases, note consistency of H3.3-ΔN -positive bands in chromosomes from the same metaphase plate or from different cells. In (**C**) a metaphase cytospin of HUVEC cell was stained for DNA (C, DAPI), expresses H3.3-ΔN (**C′**) and was immunostained for H3K27me3 (**C′′**); overlay of DAPI and H3.3-ΔN in (**C′′′**); subsequently the metaphase plate was hybridized to localize HSAX (**C′′′′**). With this procedure, it is possible to discriminate between the active and inactive X chromosomes (Xa and Xi), as H3K27me3 is enriched at Xi. The arrowhead in (**C′**) points to the H3.3-ΔN bands visible in the Xa whereas the arrow points to the position of the Xi where almost no signal is visible. Single confocal SIM section of metaphase of a Hela cell co-expressing H3.1 (**D**) and H3.3-ΔN (**D′**). Note discrete bands visible in H3.3-ΔN whereas no distinct banding pattern is seen for H3.1 expression (**D–D′′**).

followed by incubation in physiological buffer and in the transcription reaction buffer at 33 °C for 30 min, and stopped by immersion into ice-cold PBS. Incorporated transcripts were detected using immunofluorescent procedure as outlined below. A monoclonal anti-BrdUTP antibody (1:100; Roche) known to cross-react with BrUTP and a secondary FITC-labeled sheep anti-mouse polyclonal antibody (1:100; Amersham) were used to detect transcripts.

For studying chromosomes 0.1 μg/ml colcemid was added to cells in growth media for 2 h. Cells were briefly rinsed in PBS, scraped off and incubated in hypotonic solution (0.56% KCl in distilled water) at 37 °C for 10 min. Cells were quickly transferred onto adhesive glass slides (Superfrost, VWR) and subjected to cytospin centrifugation (Cytopspin 4, Shandon) at 800 rpm for 5 min. Thereafter, cells were fixed in 4% PFA in PBS for 20 min and washed in PBS. Cells were either used for further treatments or counterstained for DNA using either DAPI or quinacrine mustard for Q-banding.

Comparison of H3.3-ΔN and full-length H3.3 expression

In order to check for possible differences in the expression patterns between the two constructs we (1) generated a stable Hela cell line expressing H3.3-ΔN (**Fig. 1A′**) where the full-length construct was transiently co-expressed (**Fig. 1A′′**) and (2) transiently co-expressed both constructs in Hela cells (**Fig. 1C and C′**). The expression patterns of both constructs strongly co-localized in interphase nuclei seen by visual inspection (**Fig. 1A′′′ and C′′**). Measurement of Spearman's co-localization coefficient resulted in $r = 0.887$ (case 1) and $r = 0.914$ (case 2) confirming the highly significant signal overlap. Co-localization was furthermore observed in the conspicuous H3.3-specific banding pattern (**Fig. 1B–B′′′, D–D′′**) found on mitotic chromosomes. Subtle differences in localization of the two constructs might be present at centromeric sites which is subject of ongoing studies.

Immunofluorescence detection

After the transfection procedure cells were permeabilized with 0.5% Triton X100 for 5 min at room temperature. Cells were then briefly washed several times with PBS, and unspecific binding was reduced by incubation in PBSB (PBS supplemented with 1% bovine serum) for 20 min at 37 °C in a moist chamber. Subsequently, cells were immersed in primary antibodies diluted in PBSB for 1 h at 37 °C. Thereafter cells were washed 3× 30 min in PBST (PBS supplemented with 0.05% Tween20) and incubated in secondary antibodies diluted in PBSB for 30 min at 37 °C. Cells were washed 3× 30 min in PBST, counterstained with DAPI (Sigma) or quinacrine mustard (Sigma), and coverslips were mounted in Citifluor antifading mounting solution (Agar Scientific).

Primary antibodies used were: monoclonal anti- HIRA[68] (1:10; mixture of monoclonal antibodies WC19, WC117, WC119); rabbit polyclonal anti-H3K27me3 (1:1000; Upstate 07–449); monoclonal anti- SC-35 (1:2000; Sigma S4045); monoclonal anti- H3K4me2 and -me3 -specific (1:500; Abcam ab6000). Secondary antibodies were goat anti-mouse Alexa488 and goat anti-rabbit Alexa488 (1:1000; Life Technologies).

FISH and H3.3 expression

The protocol essentially follows reference 69. For the detection of HSA6 in interphase nuclei expressing H3.3-ΔN the FISH procedure followed the transfection of cells. Briefly, RNA was digested with RNase A and after washes in 2× SSC proteins were digested by incubation in 0.1% pepsin for 1 min. After thorough washes in 2× SSC cells were post-fixed in 4% PFA, washed again in 2× SSC and dried after immersion in ascending concentrations of ethanol. Two μl of a commercial HSA6-specific whole chromosome painting probe labeled with digoxigenin (Chromotrax T116) were mixed with 4.7 μl of the supplied hybridization buffer. The hybridization mix was placed onto the coverslip which was put upside down onto a glass slide. Probe and cells were allowed to denature simultaneously at 85 °C for 7 min and were left for annealing at 37 °C overnight. Stringency washes were performed using 2× SSC at 72 °C for 2 min followed by 4× SSCT (2× SSC supplemented with 0.05% Tween20) at room temperature. The labeled probes were detected according to the immunofluorescence protocol above using a FITC labeled sheep anti-digoxigenin antibody (1:200; Roche). Cells were counterstained with DAPI and mounted in Citifluor. By this procedure the H3.3-ΔN intensity was significantly reduced after FISH. However the retained intensity was sufficient to record images. For the co-localization of H3.3-ΔN and H3K27me3 with HSAX on metaphase chromosomes most H3.3-ΔN signal was lost after FISH and therefore a consecutive approach was applied. After transfection immunofluorescence detection was performed as described above. Images of suitable metaphase plates were taken, their position on the *x-y* table was recorded and after FISH the positions were relocated. FISH was performed as above except that protein digestion was reduced using 0.01% pepsin for 3 min, and the first stringency wash was performed with 50% formamide in 2× SSC at 42 °C for 3× 10 min. 3 μl

of a commercially available biotin-labeled, HSAX-specific whole chromosome painting probe (Cambio; 1066-XB) were mixed with 7 μl of the supplied hybridization buffer. The probes were detected using rhodamine-labeled avidin (1:200; Vector) before applying DAPI counterstaining and mounting in Citifluor.

Fluorescence microscopy

Wide-field fluorescence microscopy images were captured with an Eclipse800 upright epifluorescence microscope equipped with a 100× NA 1.4 PlanApo lens and a DS-Ri1 digital camera (Nikon). Images were recorded using NIS elements Br software (Nikon) and saved in either JPEG or TIFF formats. Confocal image stacks were obtained with a LSM510 confocal scanning microscope fitted with a 100× NA 1.4 PlanApo lens (Zeiss). Image stacks were recorded with LSM software and stored in.lsm format.

Structured illumination imaging

Stacks of SIM images were recorded on a Zeiss Elyra PS.1 system equipped with an Andor iXon 885 EMCCD camera. A 63× PlanApo M27 oil immersion lens with a NA 1.4 and diode laser lines 405 nm (DAPI), 488 nm (YFP), and 561 nm (mCherry) were used. SIM image stacks were acquired with grid distances of 42 μm at 3 angles (*z*-distance 90 μm). The ZEN software package (Zeiss) was used for computational reconstruction of superresolution images with lateral resolution of 100 nm and axial resolution of 300 nm. Channel registration was achieved by applying parameters obtained from calibration measurements using fluorescent microspheres of 0.2 μm diameter (TetraSpeck, Life Technologies). Data series were stored in .lsm format and exported as single TIFF file per optical section when needed.

Image analysis

For non-SIM images the channels of multicolor images were aligned using Adobe Photoshop software. For compensation of color offset the image planes were corrected with values specific of the microscope equipment as obtained by calibration using 0.2 μm fluorescent microspheres (TetraSpeck, Life Technologies). Grey value profiles were made with ZEN software (Zeiss) using freehand mode. Co-localization measurement was done by calculation of Pearson's and Spearman's correlation coefficients using PSC co-localization plug-in[70] in ImageJ software.[71] Co-localization measurements were either done over the whole nucleus (a region-of-interest was defined including the entire nucleus) or in areas of eu- or heterochromatin. In the latter case the areas were manually selected based on DAPI staining intensities excluding nucleoli and other chromatin-free nuclear compartments. In both cases, a user-set threshold was applied to subtract background intensity noise in a selected region-of-interest. In the case of stacks of SIM sections the measurements were made in single optical slices. Scatterplots for red and green channels of SIM images were produced with the PSC plug-in. The outlines of chromosome 6 territories were defined on 8-bit inverted images using the freely available Gold-Plug-ins Topo-Detect, Topo-Select Points, and Topo-Intensity for Ellipse software package (Vidito) as in.[72] As result isolines of intensities were produced which delineate the border of the signal obtained after FISH to detect chromosome 6 territories.

Disclosure of Potential Conflicts of Interest

No potential conflict of interest was disclosed.

Acknowledgments

We are grateful to Kahmi Ahmad for providing the H3.3 clones and to Peter D Adams (Fox Chase Cancer Center, Philadelphia) for providing the HIRA antibodies. We are indebted to Jaques Paysan, Zeiss, for expert help in operation of the SIM microscope. We thank Renate Erhart for expert help in producing stable cell lines.

References

1. Schwartz BE, Ahmad K. Transcriptional activation triggers deposition and removal of the histone variant H3.3. Genes Dev 2005; 19:804-14; PMID:15774717; http://dx.doi.org/10.1101/gad.1259805
2. Ahmad K, Henikoff S. The histone variant H3.3 marks active chromatin by replication-independent nucleosome assembly. Mol Cell 2002; 9:1191-200; PMID:12086617; http://dx.doi.org/10.1016/S1097-2765(02)00542-7
3. Frank D, Doenecke D, Albig W. Differential expression of human replacement and cell cycle dependent H3 histone genes. Gene 2003; 312:135-43; PMID:12909349; http://dx.doi.org/10.1016/S0378-1119(03)00609-7
4. Piña B, Suau P. Changes in histones H2A and H3 variant composition in differentiating and mature rat brain cortical neurons. Dev Biol 1987; 123:51-8; PMID:3622934; http://dx.doi.org/10.1016/0012-1606(87)90426-X
5. Janicki SM, Tsukamoto T, Salghetti SE, Tansey WP, Sachidanandam R, Prasanth KV, Ried T, Shav-Tal Y, Bertrand E, Singer RH, et al. From silencing to gene expression: real-time analysis in single cells. Cell 2004; 116:683-98; PMID:15006351; http://dx.doi.org/10.1016/S0092-8674(04)00171-0
6. Tamura T, Smith M, Kanno T, Dasenbrock H, Nishiyama A, Ozato K. Inducible deposition of the histone variant H3.3 in interferon-stimulated genes. J Biol Chem 2009; 284:12217-25; PMID:19244243; http://dx.doi.org/10.1074/jbc.M805651200
7. Sutcliffe EL, Parish IA, He YQ, Juelich T, Tierney ML, Rangasamy D, Milburn PJ, Parish CR, Tremethick DJ, Rao S. Dynamic histone variant exchange accompanies gene induction in T cells. Mol Cell Biol 2009; 29:1972-86; PMID:19158270; http://dx.doi.org/10.1128/MCB.01590-08
8. McKittrick E, Gafken PR, Ahmad K, Henikoff S. Histone H3.3 is enriched in covalent modifications associated with active chromatin. Proc Natl Acad Sci U S A 2004; 101:1525-30; PMID:14732680; http://dx.doi.org/10.1073/pnas.0308092100
9. Ray-Gallet D, Woolfe A, Vassias I, Pellentz C, Lacoste N, Puri A, Schultz DC, Pchelintsev NA, Adams PD, Jansen LE, et al. Dynamics of histone H3 deposition in vivo reveal a nucleosome gap-filling mechanism for H3.3 to maintain chromatin integrity. Mol Cell 2011; 44:928-41; PMID:22195966; http://dx.doi.org/10.1016/j.molcel.2011.12.006
10. Corpet A, Olbrich T, Gwerder M, Fink D, Stucki M. Dynamics of histone H3.3 deposition in proliferating and senescent cells reveals a DAXX-dependent targeting to PML-NBs important for pericentromeric heterochromatin organization. Cell Cycle 2014; 13:249-67; PMID:24200965; http://dx.doi.org/10.4161/cc.26988
11. Drané P, Ouararhni K, Depaux A, Shuaib M, Hamiche A. The death-associated protein DAXX is a novel histone chaperone involved in the replication-independent deposition of H3.3. Genes Dev 2010; 24:1253-65; PMID:20504901; http://dx.doi.org/10.1101/gad.566910
12. Hake SB, Garcia BA, Kauer M, Baker SP, Shabanowitz J, Hunt DF, Allis CD. Serine 31 phosphorylation of histone variant H3.3 is specific to regions bordering centromeres in metaphase chromosomes. Proc Natl Acad Sci U S A 2005; 102:6344-9; PMID:15851689; http://dx.doi.org/10.1073/pnas.0502413102
13. Santenard A, Ziegler-Birling C, Koch M, Tora L, Bannister AJ, Torres-Padilla ME. Heterochromatin formation in the mouse embryo requires critical residues of the histone variant H3.3. Nat Cell Biol 2010; 12:853-62; PMID:20676102; http://dx.doi.org/10.1038/ncb2089
14. Lewis PW, Elsaesser SJ, Noh KM, Stadler SC, Allis CD. Daxx is an H3.3-specific histone chaperone and cooperates with ATRX in replication-independent chromatin assembly at telomeres. Proc Natl Acad Sci U S A 2010; 107:14075-80; PMID:20651253; http://dx.doi.org/10.1073/pnas.1008850107
15. Wong LH, McGhie JD, Sim M, Anderson MA, Ahn S, Hannan RD, George AJ, Morgan KA, Mann JR, Choo KH. ATRX interacts with H3.3 in maintaining telomere structural integrity in pluripotent embryonic stem cells. Genome Res 2010; 20:351-60; PMID:20110566; http://dx.doi.org/10.1101/gr.101477.109
16. Goldberg AD, Banaszynski LA, Noh KM, Lewis PW, Elsaesser SJ, Stadler S, Dewell S, Law M, Guo X, Li X, et al. Distinct factors control histone variant H3.3 localization at specific genomic regions. Cell 2010; 140:678-91; PMID:20211137; http://dx.doi.org/10.1016/j.cell.2010.01.003

17. Wirbelauer C, Bell O, Schübeler D. Variant histone H3.3 is deposited at sites of nucleosomal displacement throughout transcribed genes while active histone modifications show a promoter-proximal bias. Genes Dev 2005; 19:1761-6; PMID:16077006; http://dx.doi.org/10.1101/gad.347705
18. Mito Y, Henikoff JG, Henikoff S. Genome-scale profiling of histone H3.3 replacement patterns. Nat Genet 2005; 37:1090-7; PMID:16155569; http://dx.doi.org/10.1038/ng1637
19. Delbarre E, Jacobsen BM, Reiner AH, Sørensen AL, Küntziger T, Collas P. Chromatin environment of histone variant H3.3 revealed by quantitative imaging and genome-scale chromatin and DNA immunoprecipitation. Mol Biol Cell 2010; 21:1872-84; PMID:20375147; http://dx.doi.org/10.1091/mbc.E09-09-0839
20. Chen P, Zhao J, Wang Y, Wang M, Long H, Liang D, Huang L, Wen Z, Li W, Li X, et al. H3.3 actively marks enhancers and primes gene transcription via opening higher-ordered chromatin. Genes Dev 2013; 27:2109-24; PMID:24065740; http://dx.doi.org/10.1101/gad.222174.113
21. Chow CM, Georgiou A, Szutorisz H, Maia e Silva A, Pombo A, Barahona I, Dargelos E, Canzonetta C, Dillon N. Variant histone H3.3 marks promoters of transcriptionally active genes during mammalian cell division. EMBO Rep 2005; 6:354-60; PMID:15776021; http://dx.doi.org/10.1038/sj.embor.7400366
22. Pchelintsev NA, McBryan T, Rai TS, van Tuyn J, Ray-Gallet D, Almouzni G, Adams PD. Placing the HIRA histone chaperone complex in the chromatin landscape. Cell Rep 2013; 3:1012-9; PMID:23602572; http://dx.doi.org/10.1016/j.celrep.2013.03.026
23. Jin C, Felsenfeld G. Nucleosome stability mediated by histone variants H3.3 and H2A.Z. Genes Dev 2007; 21:1519-29; PMID:17575053; http://dx.doi.org/10.1101/gad.1547707
24. Jin C, Felsenfeld G. Distribution of histone H3.3 in hematopoietic cell lineages. Proc Natl Acad Sci U S A 2006; 103:574-9; PMID:16407103; http://dx.doi.org/10.1073/pnas.0509974103
25. Hake SB, Garcia BA, Duncan EM, Kauer M, Dellaire G, Shabanowitz J, Bazett-Jones DP, Allis CD, Hunt DF. Expression patterns and post-translational modifications associated with mammalian histone H3 variants. J Biol Chem 2006; 281:559-68; PMID:16267050; http://dx.doi.org/10.1074/jbc.M509266200
26. Tagami H, Ray-Gallet D, Almouzni G, Nakatani Y. Histone H3.1 and H3.3 complexes mediate nucleosome assembly pathways dependent or independent of DNA synthesis. Cell 2004; 116:51-61; PMID:14718166; http://dx.doi.org/10.1016/S0092-8674(03)01064-X
27. Ray-Gallet D, Quivy JP, Scamps C, Martini EM, Lipinski M, Almouzni G. HIRA is critical for a nucleosome assembly pathway independent of DNA synthesis. Mol Cell 2002; 9:1091-100; PMID:12049744; http://dx.doi.org/10.1016/S1097-2765(02)00526-9
28. Skene PJ, Henikoff S. Histone variants in pluripotency and disease. Development 2013; 140:2513-24; PMID:23715545; http://dx.doi.org/10.1242/dev.091439
29. Couldrey C, Carlton MB, Nolan PM, Colledge WH, Evans MJ. A retroviral gene trap insertion into the histone 3.3A gene causes partial neonatal lethality, stunted growth, neuromuscular deficits and male sub-fertility in transgenic mice. Hum Mol Genet 1999; 8:2489-95; PMID:10556297; http://dx.doi.org/10.1093/hmg/8.13.2489
30. Tang MC, Jacobs SA, Wong LH, Mann JR. Conditional allelic replacement applied to genes encoding the histone variant H3.3 in the mouse. Genesis 2013; 51:142-6; PMID:23315948; http://dx.doi.org/10.1002/dvg.22366
31. Bush KM, Yuen BT, Barrilleaux BL, Riggs JW, O'Geen H, Cotterman RF, Knoepfler PS. Endogenous mammalian histone H3.3 exhibits chromatin-related functions during development. Epigenetics Chromatin 2013; 6:7; PMID:23570311; http://dx.doi.org/10.1186/1756-8935-6-7
32. Sakai A, Schwartz BE, Goldstein S, Ahmad K. Transcriptional and developmental functions of the H3.3 histone variant in Drosophila. Curr Biol 2009; 19:1816-20; PMID:19781938; http://dx.doi.org/10.1016/j.cub.2009.09.021
33. Hödl M, Basler K. Transcription in the absence of histone H3.3. Curr Biol 2009; 19:1221-6; PMID:19523831; http://dx.doi.org/10.1016/j.cub.2009.05.048
34. Ng RK, Gurdon JB. Epigenetic memory of an active gene state depends on histone H3.3 incorporation into chromatin in the absence of transcription. Nat Cell Biol 2008; 10:102-9; PMID:18066050; http://dx.doi.org/10.1038/ncb1674
35. Cox SG, Kim H, Garnett AT, Medeiros DM, An W, Crump JG. An essential role of variant histone H3.3 for ectomesenchyme potential of the cranial neural crest. PLoS Genet 2012; 8:e1002938; PMID:23028350; http://dx.doi.org/10.1371/journal.pgen.1002938
36. Banaszynski LA, Wen D, Dewell S, Whitcomb SJ, Lin M, Diaz N, Elsässer SJ, Chapgier A, Goldberg AD, Canaani E, et al. Hira-dependent histone H3.3 deposition facilitates PRC2 recruitment at developmental loci in ES cells. Cell 2013; 155:107-20; PMID:24074864; http://dx.doi.org/10.1016/j.cell.2013.08.061
37. Lin CJ, Conti M, Ramalho-Santos M. Histone variant H3.3 maintains a decondensed chromatin state essential for mouse preimplantation development. Development 2013; 140:3624-34; PMID:23903189; http://dx.doi.org/10.1242/dev.095513
38. Szenker E, Lacoste N, Almouzni G. A developmental requirement for HIRA-dependent H3.3 deposition revealed at gastrulation in Xenopus. Cell Rep 2012; 1:730-40; PMID:22813747; http://dx.doi.org/10.1016/j.celrep.2012.05.006
39. Torres-Padilla ME, Bannister AJ, Hurd PJ, Kouzarides T, Zernicka-Goetz M. Dynamic distribution of the replacement histone variant H3.3 in the mouse oocyte and preimplantation embryos. Int J Dev Biol 2006; 50:455-61; PMID:16586346
40. Akiyama T, Suzuki O, Matsuda J, Aoki F. Dynamic replacement of histone H3 variants reprograms epigenetic marks in early mouse embryos. PLoS Genet 2011; 7:e1002279; PMID:21998593; http://dx.doi.org/10.1371/journal.pgen.1002279
41. Filipescu D, Szenker E, Almouzni G. Developmental roles of histone H3 variants and their chaperones. Trends Genet 2013; 29:630-40; PMID:23830582; http://dx.doi.org/10.1016/j.tig.2013.06.002
42. Banaszynski LA, Allis CD, Lewis PW. Histone variants in metazoan development. Dev Cell 2010; 19:662-74; PMID:21074717; http://dx.doi.org/10.1016/j.devcel.2010.10.014
43. Orsi GA, Couble P, Loppin B. Epigenetic and replacement roles of histone variant H3.3 in reproduction and development. Int J Dev Biol 2009; 53:231-43; PMID:19412883; http://dx.doi.org/10.1387/ijdb.082653go
44. Barrero CA, Perez-Leal O, Aksoy M, Moncada C, Ji R, Lopez Y, Mallilankaraman K, Madesh M, Criner GJ, Kelsen SG, et al. Histone 3.3 participates in a self-sustaining cascade of apoptosis that contributes to the progression of chronic obstructive pulmonary disease. Am J Respir Crit Care Med 2013; 188:673-83; PMID:23924319; http://dx.doi.org/10.1164/rccm.201302-0342OC
45. Sturm D, Witt H, Hovestadt V, Khuong-Quang DA, Jones DT, Konermann C, Pfaff E, Tönjes M, Sill M, Bender S, et al. Hotspot mutations in H3F3A and IDH1 define distinct epigenetic and biological subgroups of glioblastoma. Cancer Cell 2012; 22:425-37; PMID:23079654; http://dx.doi.org/10.1016/j.ccr.2012.08.024
46. Schwartzentruber J, Korshunov A, Liu XY, Jones DT, Pfaff E, Jacob K, Sturm D, Fontebasso AM, Quang DA, Tönjes M, et al. Driver mutations in histone H3.3 and chromatin remodelling genes in paediatric glioblastoma. Nature 2012; 482:226-31; PMID:22286061; http://dx.doi.org/10.1038/nature10833
47. Joseph CG, Hwang H, Jiao Y, Wood LD, Kinde I, Wu J, Mandahl N, Luo J, Hruban RH, Diaz LA Jr., et al. Exomic analysis of myxoid liposarcomas, synovial sarcomas, and osteosarcomas. Genes Chromosomes Cancer 2014; 53:15-24; PMID:24190505; http://dx.doi.org/10.1002/gcc.22114
48. Wu G, Broniscer A, McEachron TA, Lu C, Paugh BS, Becksfort J, Qu C, Ding L, Huether R, Parker M, et al.; St. Jude Children's Research Hospital–Washington University Pediatric Cancer Genome Project. Somatic histone H3 alterations in pediatric diffuse intrinsic pontine gliomas and non-brainstem glioblastomas. Nat Genet 2012; 44:251-3; PMID:22286216; http://dx.doi.org/10.1038/ng.1102
49. Behjati S, Tarpey PS, Presneau N, Scheipl S, Pillay N, Van Loo P, Wedge DC, Cooke SL, Gundem G, Davies H, et al. Distinct H3F3A and H3F3B driver mutations define chondroblastoma and giant cell tumor of bone. Nat Genet 2013; 45:1479-82; PMID:24162739; http://dx.doi.org/10.1038/ng.2814
50. Ting DT, Lipson D, Paul S, Brannigan BW, Akhavanfard S, Coffman EJ, Contino G, Deshpande V, Iafrate AJ, Letovsky S, et al. Aberrant overexpression of satellite repeats in pancreatic and other epithelial cancers. Science 2011; 331:593-6; PMID:21233348; http://dx.doi.org/10.1126/science.1200801
51. Salomoni P. The PML-Interacting Protein DAXX: Histone Loading Gets into the Picture. Front Oncol 2013; 3:152; PMID:23760585
52. Yuen BT, Knoepfler PS. Histone H3.3 mutations: a variant path to cancer. Cancer Cell 2013; 24:567-74; PMID:24229707; http://dx.doi.org/10.1016/j.ccr.2013.09.015
53. Delbarre E, Ivanauskiene K, Küntziger T, Collas P. DAXX-dependent supply of soluble (H3.3-H4) dimers to PML bodies pending deposition into chromatin. Genome Res 2013; 23:440-51; PMID:23222847; http://dx.doi.org/10.1101/gr.142703.112
54. Visser AE, Eils R, Jauch A, Little G, Bakker PJM, Cremer T, Aten JA. Spatial distributions of early and late replicating chromatin in interphase chromosome territories. Exp Cell Res 1998; 243:398-407; PMID:9743599; http://dx.doi.org/10.1006/excr.1998.4144
55. Albiez H, Cremer M, Tiberi C, Vecchio L, Schermelleh L, Dittrich S, Küpper K, Joffe B, Thormeyer T, von Hase J, et al. Chromatin domains and the interchromatin compartment form structurally defined and functionally interacting nuclear networks. Chromosome Res 2006; 14:707-33; PMID:17115328; http://dx.doi.org/10.1007/s10577-006-1086-x
56. Shopland LS, Johnson CV, Byron M, McNeil J, Lawrence JB. Clustering of multiple specific genes and gene-rich R-bands around SC-35 domains: evidence for local euchromatic neighborhoods. J Cell Biol 2003; 162:981-90; PMID:12975345; http://dx.doi.org/10.1083/jcb.200303131

57. Brown JM, Green J, das Neves RP, Wallace HA, Smith AJ, Hughes J, Gray N, Taylor S, Wood WG, Higgs DR, et al. Association between active genes occurs at nuclear speckles and is modulated by chromatin environment. J Cell Biol 2008; 182:1083-97; PMID:18809724; http://dx.doi.org/10.1083/jcb.200803174
58. Markaki Y, Gunkel M, Schermelleh L, Beichmanis S, Neumann J, Heidemann M, Leonhardt H, Eick D, Cremer C, Cremer T. Functional nuclear organization of transcription and DNA replication: a topographical marriage between chromatin domains and the interchromatin compartment. Cold Spring Harb Symp Quant Biol 2010; 75:475-92; PMID:21467142; http://dx.doi.org/10.1101/sqb.2010.75.042
59. Hake SB, Allis CD. Histone H3 variants and their potential role in indexing mammalian genomes: the "H3 barcode hypothesis". Proc Natl Acad Sci U S A 2006; 103:6428-35; PMID:16571659; http://dx.doi.org/10.1073/pnas.0600803103
60. Dunleavy EM, Almouzni G, Karpen GH. H3.3 is deposited at centromeres in S phase as a placeholder for newly assembled CENP-A in G_1 phase. Nucleus 2011; 2:146-57; PMID:21738837; http://dx.doi.org/10.4161/nucl.2.2.15211
61. Gustafsson MG. Surpassing the lateral resolution limit by a factor of two using structured illumination microscopy. J Microsc 2000; 198:82-7; PMID:10810003; http://dx.doi.org/10.1046/j.1365-2818.2000.00710.x
62. Markaki Y, Smeets D, Fiedler S, Schmid VJ, Schermelleh L, Cremer T, Cremer M. The potential of 3D-FISH and super-resolution structured illumination microscopy for studies of 3D nuclear architecture: 3D structured illumination microscopy of defined chromosomal structures visualized by 3D (immuno)-FISH opens new perspectives for studies of nuclear architecture. Bioessays 2012; 34:412-26; PMID:22508100; http://dx.doi.org/10.1002/bies.201100176
63. Lanctôt C, Cheutin T, Cremer M, Cavalli G, Cremer T. Dynamic genome architecture in the nuclear space: regulation of gene expression in three dimensions. Nat Rev Genet 2007; 8:104-15; PMID:17230197; http://dx.doi.org/10.1038/nrg2041
64. Schöfer C, Weipoltshammer K. Gene dynamics and nuclear architecture during differentiation. Differentiation 2008; 76:41-56; PMID:17908252
65. Hu Y, Plutz M, Belmont AS. Hsp70 gene association with nuclear speckles is Hsp70 promoter specific. J Cell Biol 2010; 191:711-9; PMID:21059845; http://dx.doi.org/10.1083/jcb.201004041
66. Croft JA, Bridger JM, Boyle S, Perry P, Teague P, Bickmore WA. Differences in the localization and morphology of chromosomes in the human nucleus. J Cell Biol 1999; 145:1119-31; PMID:10366586; http://dx.doi.org/10.1083/jcb.145.6.1119
67. Hozák P, Cook PR, Schöfer C, Mosgöller W, Wachtler F. Site of transcription of ribosomal RNA and intranucleolar structure in HeLa cells. J Cell Sci 1994; 107:639-48; PMID:8207086
68. Hall C, Nelson DM, Ye X, Baker K, DeCaprio JA, Seeholzer S, Lipinski M, Adams PD. HIRA, the human homologue of yeast Hir1p and Hir2p, is a novel cyclin-cdk2 substrate whose expression blocks S-phase progression. Mol Cell Biol 2001; 21:1854-65; PMID:11238922; http://dx.doi.org/10.1128/MCB.21.5.1854-1865.2001
69. Philimonenko AA, Janacek J, Snyers L, Almeder M, Berger W, Schmidt W, Schöfer C, Hozák P, Weipoltshammer K. Chromosomal dynamics of cell cycle regulator gene p21 during transcriptional activation. J Struct Biol 2011; 173:382-90; PMID:20974257; http://dx.doi.org/10.1016/j.jsb.2010.10.010
70. French AP, Mills S, Swarup R, Bennett MJ, Pridmore TP. Colocalization of fluorescent markers in confocal microscope images of plant cells. Nat Protoc 2008; 3:619-28; PMID:18388944; http://dx.doi.org/10.1038/nprot.2008.31
71. Rasband WS. ImageJ [Internet]. Bethesda, MD: National Institutes of Health: c1997-2009 [cited 2014 August 25] Available from: http://rsb.info.nih.gov/ij/
72. Schöfer C, Janácek J, Weipoltshammer K, Pourani J, Hozák P. Mapping of cellular compartments based on ultrastructural immunogold labeling. J Struct Biol 2004;